iScience

CellPress
OPEN ACCESS

Article

A negative-work knee energy harvester based on homo-phase transfer for wearable monitoring devices

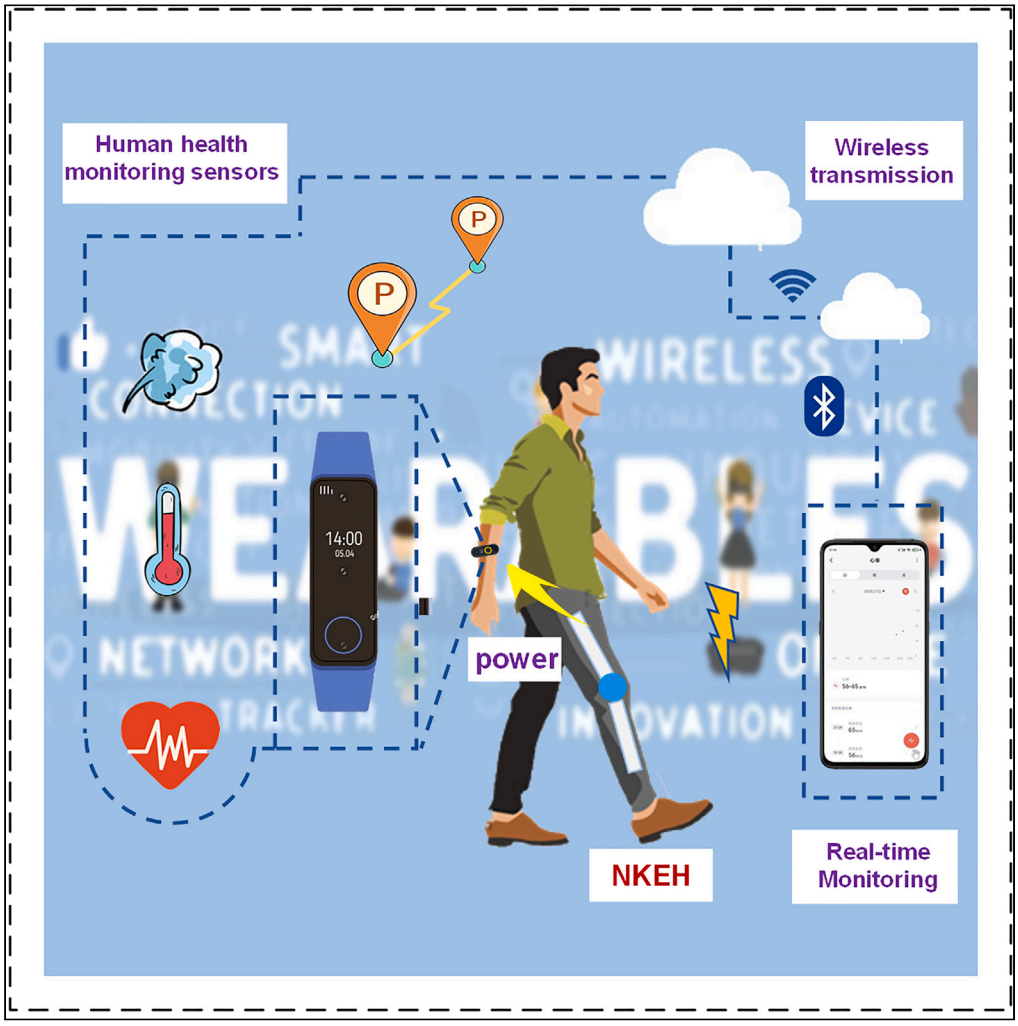

Hexiang Zhang, Hao Wang, Zutao Zhang, Yajia Pan, Xiao Luo

zzt@swjtu.edu.cn (Z.Z.)
yjpan@home.swjtu.edu.cn (Y.P.)

Highlights

A negative-work knee energy harvester applied to health monitoring is proposed

Only negative muscle work was harvested based on homo-phase transfer mechanism

The harvester can produce 12.95 mW power while installed on a human

Zhang et al., iScience *26*, 107011
July 21, 2023
https://doi.org/10.1016/j.isci.2023.107011

iScience

CellPress
OPEN ACCESS

Article

A negative-work knee energy harvester based on homo-phase transfer for wearable monitoring devices

Hexiang Zhang,[1,2] Hao Wang,[1,2] Zutao Zhang,[1,2,3,*] Yajia Pan,[1,*] and Xiao Luo[2]

SUMMARY

Wearable health monitoring devices can effectively capture human body information and are widely used in health monitoring, but battery life is an important bottleneck in its development. A full negative-work energy harvester based on the homo-phase transfer mechanism by analyzing human motion characteristics was proposed in this paper. The system was designed based on the homo-phase transfer mechanism, including a motion input module, gear acceleration module, energy conversion module, and electric energy storage module. The output performance in three human-level, downhill, and running states was tested, respectively. Finally, we have evaluated the feasibility of an energy harvester powering wearable health monitoring devices, and the harvester can generate 17.40 J/day power, which can satisfy the normal operation of a typical health monitoring device. This study has certain promoting significance for the development of a new generation of human health monitoring.

INTRODUCTION

In recent years, biosensors have made tremendous progress in both materials and functions.[1–3] For example, biosensors based on fiber materials have improved the permeability and comfort of devices,[4–6] while wearable sensors based on nanosheets have shown higher potential due to their high surface area ratio.[7–9] Smart wearable devices equipped with various biosensors can effectively capture human body information for health monitoring applications, greatly improving the ability of humans to resist diseases.[10–12] These electronic monitoring devices usually use batteries to provide energy. When the battery runs out, they need to be replaced or recharged regularly, which is cumbersome and affects the stability of health monitoring. Therefore, battery life has become a problem in the progress of wearable monitoring equipment.[13–15]

Human-based mechanical energy is a direct energy source for wearable health monitoring devices. Relevant studies have shown that the human body consumes hundreds or even kilowatts of energy during daily walking, while the power consumption of most health monitoring equipment is only at the milliwatt level. Thus, just a small amount of mechanical energy from a person's daily activities is sufficient to power a wearable health monitoring device.[16–18] The human body movements that can drive the biological energy harvesters include: inertial excitation, force excitation, and relative motion excitation. Among them, energy harvesters that utilize human body inertia include energy collection backpacks and eccentric rotor generators.[19] Energy harvesters that use human body force excitation include touch generators and push generators.[20] Human body relative motion excitation is generally considered as the relative motion between limbs caused by joint rotation. Compared with the previous two forms of excitation, researchers seem to pay more attention to this aspect of research and have developed various forms of energy harvesters, including knee joint energy harvesters, ankle joint energy harvesters, and hip joint energy harvesters.[21,22] The knee joint has a large range of rotation when humans walk, which can produce a considerable amount of mechanical energy. Therefore, researchers have developed various forms of knee joint energy harvesters. For instance, Yan Bai ping et al. proposed a rotating magnetostrictive design that can capture the oscillation energy of the knee during human walking. It is noteworthy that the collector still exhibited good output power under periodic oscillation and low-frequency human walking.[23] Fei Gao et al. produced a knee joint piezoelectric energy harvester that utilizes the rotation of the knee joint to bend the piezoelectric sheet, generating electricity.[24] In addition, researchers have explored energy harvesters of

[1]School of Mechanical Engineering, Southwest Jiaotong University, Chengdu 610031, P.R. China

[2]Yibin Research Institute, Southwest Jiaotong University, Yibin 644000, P.R. China

[3]Lead contact

*Correspondence: zzt@swjtu.edu.cn (Z.Z.), yjpan@home.swjtu.edu.cn (Y.P.)

https://doi.org/10.1016/j.isci.2023.107011

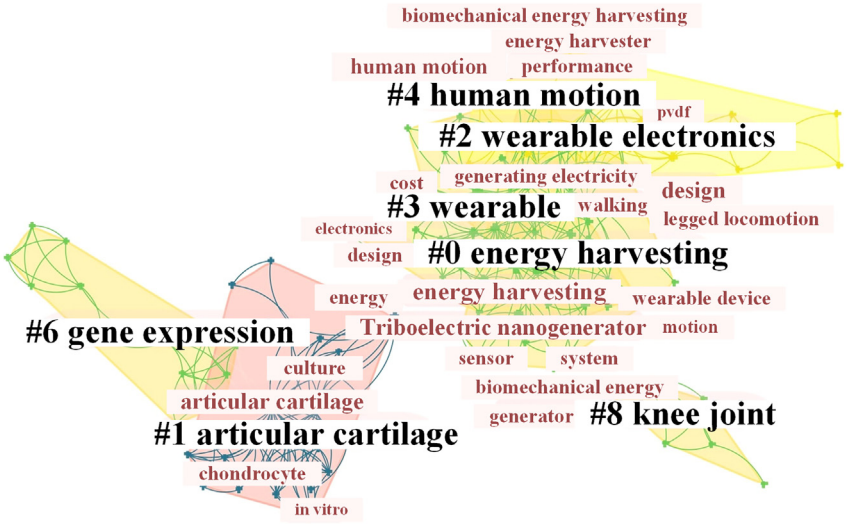

Figure 1. Hotspot analysis diagram based on CiteSpace

other joints. For example, Dai dan et al. conducted a study on the collection of hip joint kinematic energy during human walking. The experimental results showed that at a walking speed of 1.47 m/s, the voltage and output power of the electromagnetic energy generator were 1 V and 0.284 mW, respectively.[25] E. Romero et al. proposed a miniature rotating energy harvester that uses an inertial axial structure consisting of multiple permanent magnets and stacked micro-planar coils to extract electrical energy from multiple joint positions during human movement.[26]

A visual analysis of studies on human motion energy harvesting since 2010 was conducted using CiteSpace software, and the clustered view is shown in Figure 1.[27,28] It can be seen that previous studies have focused more on the output power, conversion efficiency, wearability, and conversion mechanism while ignoring the impact of the device on the metabolic consumption of the host.[29–31]

Recently, some researchers have tried to reduce metabolic consumption while generating electricity, to reduce the impact on the host by selectively harvesting the negative work of human muscles.[32–34] The positive muscle work drives the body to move, and the collection of energy at that stage increases the burden on the muscles and brings about additional metabolic consumption. The negative muscle can be imagined as the brake braking of a car system, and theoretically, harvesting energy at this phase can reduce the burden on the muscles without causing additional metabolic exertion. Therefore, in recent years, people have also conducted to allow energy harvesters to generate electricity selectively.[35–37] Some studies have used potentiometers or sensors to monitor the rotation angle of the knee joint in order to control the timing of the motor's engagement. For example, Donelan proposed a wearable knee harvester that controls the access to the generator load by using a potentiometer to detect the angle of the knee joint, a method that allows flexible control of the timing of the generator.[38] In addition, researchers have also controlled the timing of power generation through various mechanical structures to reduce the burden on the host. For example, some studies have utilized mechanical structures such as spring damping systems to replace some muscle functions, while others have used gear separation between the pendulum gear and input-output gear to control the connection of the generator.[39,40] Similarly, Shepertycky et al. use a one-way bearing and a coiled spring mechanism to make the cable intermittently connected to the generator depending on the user's gait phase.[41] Chan et al. use a roller-cable mechanism with a variable radius ratio to control the access and disconnection of the generator.[42] In addition, Liu et al. designed and compared four types of ankle joint energy harvesters, of which two designs utilized gear transmission mechanisms, and the other two designs combined spring and clutch mechanisms. These designs showed better energy harvesting performance but had more significant impacts on the human body. The design utilizing spring structures had less effect on the human body; however, it had lower energy harvesting ability. The design combining the spring and gear transmission mechanism could balance both aspects.[43]

Although some studies exist to enable energy harvesters to generate power during the negative muscle work period through sensor detection and mechanical structure design, however, these studies still have some shortcomings in practical applications. The use of sensors can detect the angle changes of joints during human movement in real time and flexibly control the working state of the harvester; the electrical power consumption of sensors and control circuits will reduce the output power of the device and affect its performance in practical applications.[38] For another passive control method that does not require sensors, some mechanical structures are used in conjunction to achieve the same function. This method avoids the sensing electronics consuming power, but the complex structure will increase the system's weight and size, bringing great inconvenience to the wearer's daily activities.[44,45] A feasible solution is to combine the biological characteristics of human movement and design a simple and effective mechanism to harvest energy from the human body without redundant or complex structures that would cause power loss and increase the burden on users. By collecting mechanical energy from the human body while reducing the user's burden, it is possible to achieve an efficient energy harvesting process.

The most important issue in this field is how to design an energy harvesting system that could generate power during the negative-work phase of human walking while meeting the requirements of small size and lightweight without affecting the wearer's activities. A full negative-work knee energy harvester (NKEH) based on the homo-phase transfer mechanism by analyzing the biological characteristics of human walking was proposed in this paper. The motion input module is engaged and disengaged by a one-way bearing corresponding to the power generation module. In the swing extension phase, the one-way bearing engages and transmits torque to drive the rotor rotation to generate electricity. In the other phases of the gait cycle, the one-way bearing disengaged, and the energy harvester uses the rotor rotation inertia to generate electricity. A rechargeable lithium battery stores the rectified and regulated electrical energy and provides power to the wearable device. Based on the biomechanics of human motion, this study uses a one-way bearing drive mechanism that does not require sensors to detect human knee swing angle and avoids additional power consumption of the potentiometer. Meanwhile, the designed harvester can fully use the rotor's rotational inertia to improve energy harvesting efficiency.

Inspired negative-work knee energy harvester

Human walking and homo-phase transfer mechanism

Understanding the kinematics of human walking is essential for designing the knee energy harvester. Human walking can be viewed as a series of periodic movements performed by the lower limbs; one of the basic units of motion is called the gait cycle. During a gait cycle, the muscles alternately do positive and negative work.[46] Figure 2A shows the swing angle and muscle work done by the knee joint during a gait cycle, and the blue part above the zero power line represents positive muscle work, and the yellow part below zero power represents negative muscle work.[40] The whole gait cycle consists of three phases: the stance phase, the swing flexion, and swing extension phase. Knee joint mainly plays a supporting role in the stance phase, the swing angle is small, and muscles basically do not work. The knee joint is responsible for lifting the leg to push human to walk in the swing flexion phase, and muscles do positive work. In the swing extension phase, the knee joint is responsible for slowing down the leg, and muscles do negative work.

This paper proposes a homo-phase transfer mechanism based on the relationship between the knee's swing angle muscles' work during each phase of human movement; the basic working mechanism is shown in Figure 2B. Using a gear train and one-way bearing transmission mechanism, the muscles do positive work in the swing flexion phase, and the knee joint rotates clockwise. The one-way bearing is disengaged, and no movement can be transferred. Correspondingly, in the swing extension phase, muscles do negative work and the knee rotates counterclockwise. Through the gear train drive, the one-way bearing engaged in this phase, transmitting motion and driving the energy harvester to generate electricity. This homo-phase transfer mechanism ensures that the generator harvests full negative muscle work in the swing extension phase and does not cause significant disturbance to the human movement.

System design

Based on the homo-phase transfer mechanism, we propose a full NKEH, which harvests the negative work done by muscles during human movement to power wearable health detection devices. The system includes a motion input module, gear acceleration module, energy conversion module, and electric energy storage module, as shown in Figure 3. The NKEH mounted at human knee joint through thigh and shank

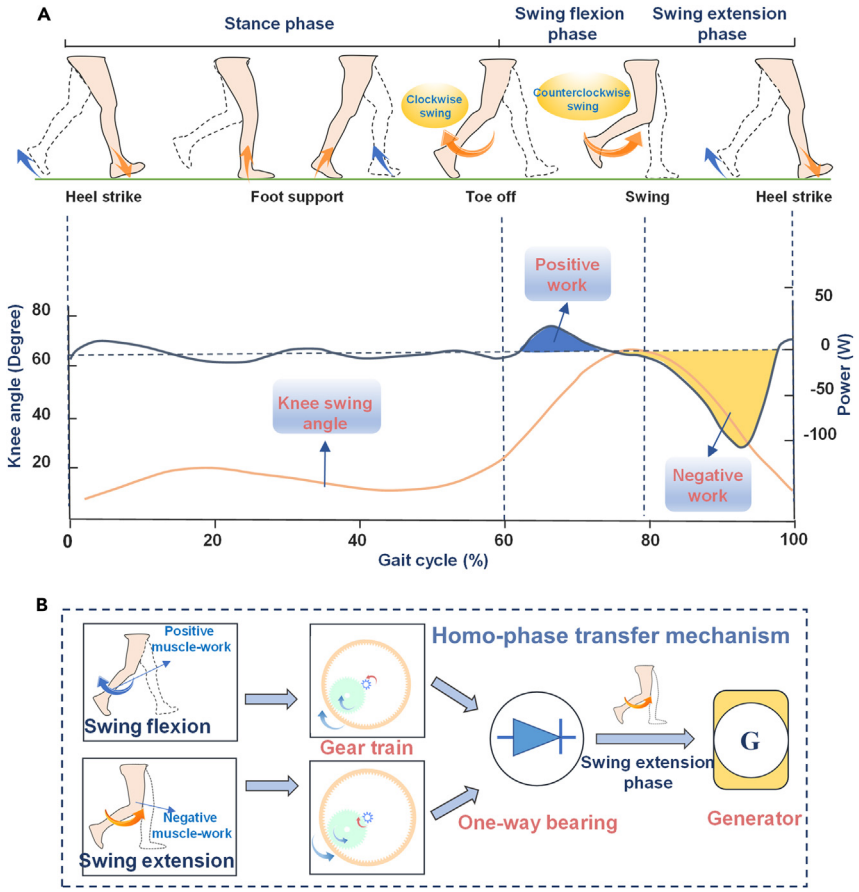

Figure 2. Human walking and homo-phase transfer mechanism

(A) Knee angle and muscle work during human walking cycle.

(B) Schematic diagram of homo-phase transfer mechanism.

wraps, and the motion input module transmits the knee motion to the energy harvester. A planetary gear train is used in the gear acceleration module to amplify the human motion input. The energy conversion module uses electromagnetic conversion to convert mechanical energy into electricity. A rechargeable lithium battery stores the rectified and regulated electrical energy and provides power to the wearable device.

Mechanical design

The installation schematic of NKEH is shown in Figure 4A. The NKEH is attached to a flexible pad, fixed to the knee joint using two linkages and straps, and does not come into direct contact with the human body, thus avoiding any potential harm to the user. The NKEH consists of a planetary gear train, a drive shaft, a one-way bearing, a rotor, a stator, bearings, a central shaft, and an end cover; the structure and compositions are shown in Figure 4B. Because the human body moves less frequently, which is not conducive to energy harvesting, this paper uses a planetary gear train to accelerate the knee oscillation speed. The planetary gear train consists of sun gear, three planetary gears, and a ring gear. Two linkages are connected to the gear ring and stator, respectively, and fixed to the thigh and calf by wraps. When the knee joint swings, the linkage drives the wheel system to rotate and transfer the body's mechanical energy to the harvester. The relevant design parameters of the gear train are shown in Table 1. To achieve homo-phase transfer, we use a one-way bearing mechanism, which engages and disengages the drive shaft according to the gait cycle phase. The stator is connected to the thigh linkage and fixed at the knee joint. Eight coils are evenly distributed on the stator and the output voltages by connecting in series. The rotor is rotated around the central axis by the driving force; eight magnets are distributed around the rotor. The design parameters of the rotor and stator are shown in Table 2.

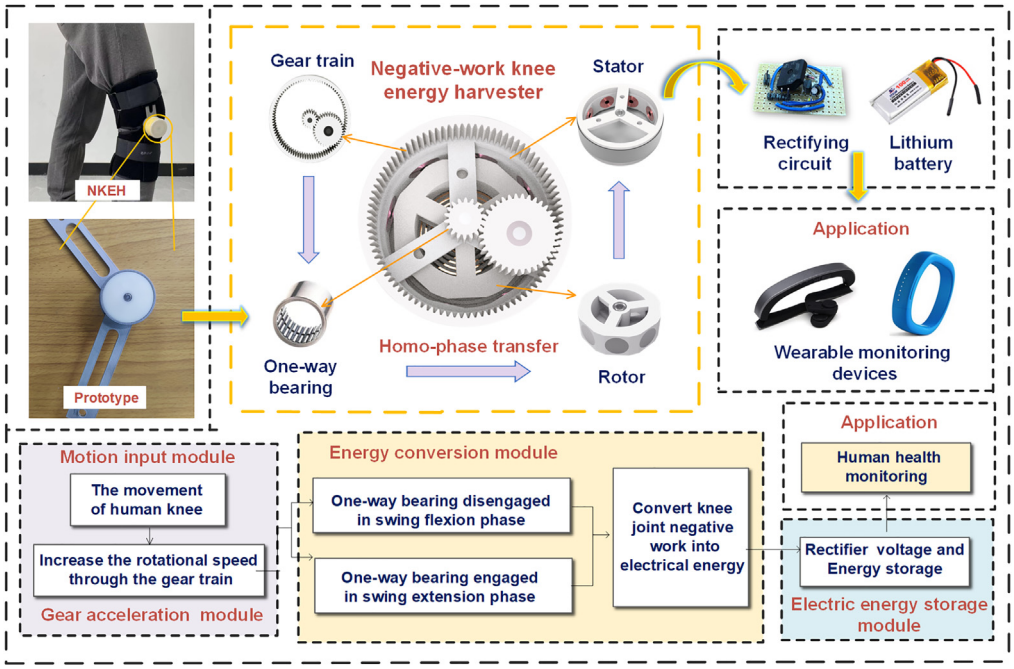

Figure 3. The general architecture of the NKEH

The proposed NKEH harvests the full knee-negative muscles work based on the homo-phase transfer mechanism; the specific working model is shown in Figure 4C. The state (i) is the swing flexion phase, where the muscles do positive work, and the knee joint rotates to drive the drive shaft counterclockwise, the one-way bearing and drive shaft are disengaged, no motion is transferred, and the energy harvester does not generate electricity. State (ii) indicates that the body is in the swing extension phase, the muscles do positive work, the drive shaft rotates clockwise, and the one-way bearing and drive shaft engaged in this direction, transferring torque, and the rotor rotates to generate current. State (iii) indicates that when the body is in the standing phase, the knee joint does not rotate and there is no mechanical energy input to the system, but the rotor keeps on rotating under the effect of rotational inertia and the device is still capable of generating electricity.

The electrical energy storage module

Since the proposed NKEH is used to harvest the knee-negative muscle work, the induced current generated by the NKEH depends on the mechanical energy input from the knee joint. The voltage obtained by the energy harvester has a high degree of instability due to the randomness of human movement. Unstable voltage is neither suitable for directly charging lithium batteries nor for powering electronic devices. For this reason, we designed a rectifier-regulator circuit to manage the power generated by the NKEH. Figure 4D shows the specific circuit components and related parameters. Firstly, the rectifier diode converts A.C. power into D.C. power. Then, the electricity is boosted by a simple and efficient PW5100 chip. Finally, after the AM1117 chip voltage stabilization process, the power is stored in a small-size lithium battery. The flow of energy transfer is shown in Figure 4E. The rectified, boosted, and regulated electrical energy powers the wearable health monitoring device.

Weight analysis of the NKEH

The proposed NKEH is worn on the human body and harvests knee-negative muscle work. Therefore, to ensure that the device is well wearable and does not interfere with human activity when worn, it is necessary to have a lightweight design of the NKEH. In this paper, the lightweight resin material is used to manufacture the main body of the harvester through 3D printing, and the linkages are made of 6061 aluminum alloy with less density, which not only ensures the strength requirements but also achieves the lightweight design requirements. Previous studies have shown that the mass of wearable devices needs to be

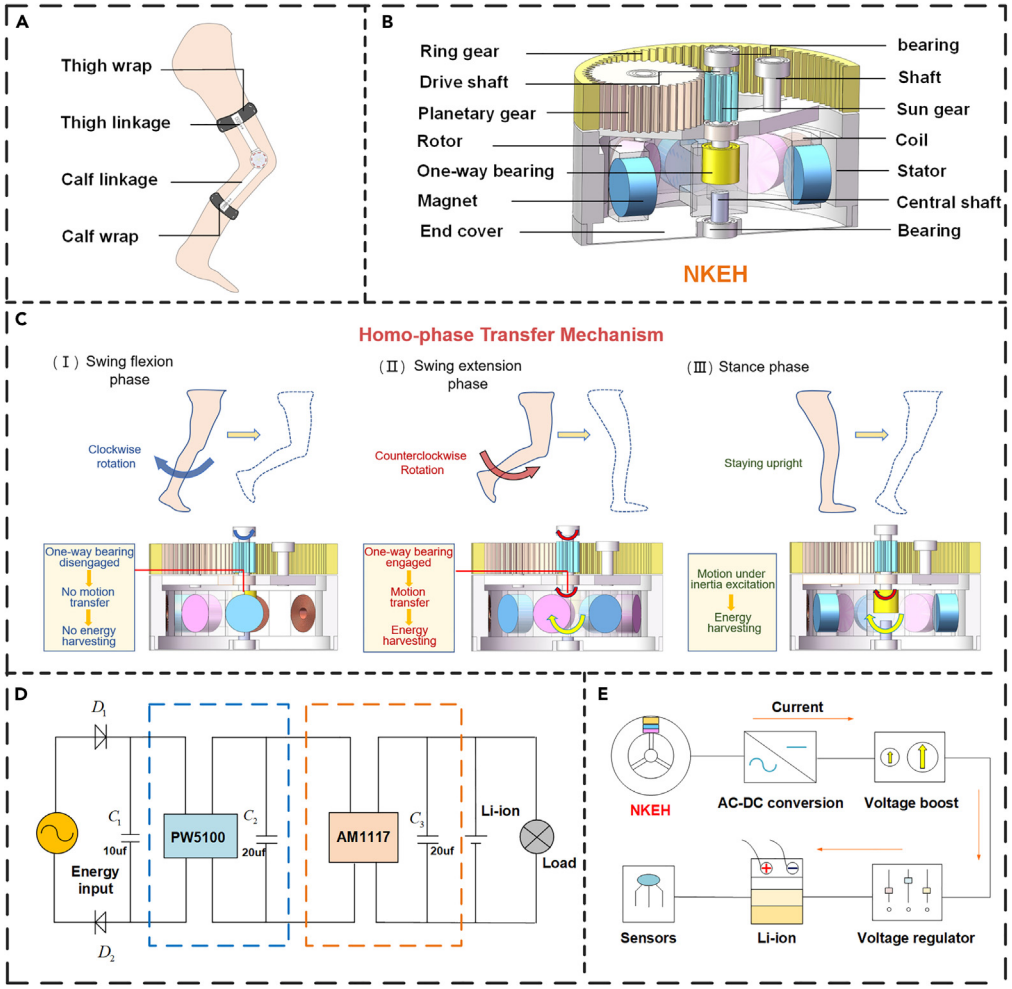

Figure 4. System composition of NKEH and working principle based on homo-phase mechanism

(A) Installation schematic of the NKEH.

(B) Structure and compositions of the NKEH.

(C) The working models based on homo-phase transfer mechanism.

(D) Voltage regulation and storage circuit.

(E) Energy transfer flowchart.

controlled at 5% of the user's own weight in order not to cause inconvenience to the user's daily activities. The mass of the proposed NKEH (with linkages) is only 186 g, which is completely within the permissible mass range for human wearers.

Table 1. Design parameters of the planetary gear train

Parameter	Value	Parameter	Value
Modulus	0.5 mm	Planetary gear teeth	40
Pressure angle	20°	Pitch diameter of planetary	20 mm
Ring gear teeth	90	Sun gear teeth	10
Pitch diameter of ring gear	45 mm	Pitch diameter of sun gear	5 mm
Outer diameter of ring gear	50 mm	Drive shaft length	22 mm
Inner diameter of bearing	3 mm	Outer diameter of bearing	6 mm

Table 2. Design parameters of the rotor and stator

Parameter	Value	Parameter	Value
Diameter (rotor)	38 mm	Turns (each coil)	690
Diameter (magnets)	10 mm	Number (coils)	8
Thickness (magnets)	5 mm	Resistance (each coil)	20 Ω
Outer diameter (stator)	50 mm	Type (magnets)	NdFeB-N50
Inner diameter (stator)	40 mm	Number (magnets)	8
Outer diameter (coils)	10 mm	Type (one-way bearing)	HF0306
Length (one-way bearing)	6 mm	Thickness (coils)	4 mm

Modeling and analysis

Gear train model and power generation

The lower frequency and amplitude of human movement result in a correspondingly small angular velocity of knee oscillation, which is not conducive to the drive for power generation. Therefore, we designed a planetary gear train to accelerate the system input, and Figure 5A demonstrates its operating schematic. The knee angular velocity is basically constant during the swing phase, and the outer side of gear ring is connected to the calf linkage. Therefore, its rotation speed ω_1 is the same as the knee rotation speed ω_0:

$$\omega_1 = \omega_0 \quad \text{(Equation 1)}$$

The planetary gear is internally meshed with the ring gear; according to the gear transmission characteristics, we can calculate the planetary gear rotational angular velocity ω_2:

$$\omega_2 = \frac{r_1}{r_2}\omega_1 = \frac{mz_1}{mz_2}\omega_1 = \frac{z_1}{z_2}\omega_1 \quad \text{(Equation 2)}$$

where m is the modulus, r_1 is the radius of the ring gear's pitch circle, z_1 is the teeth number of the ring gear, r_2 is the radius of the planetary gear's pitch circle, and z_2 is the teeth number of the planetary gear. The sun gear is externally meshed with the planetary gear, and it is possible to get the sun gear rotational angular velocity ω_3:

$$\omega_3 = \frac{r_2}{r_3}\omega_2 = \frac{mz_2}{mz_3}\omega_1 = \frac{z_2}{z_3}\omega_2 \quad \text{(Equation 3)}$$

where z_3 and r_3 are the teeth number and the radius of the pitch circle of the sun gear, respectively. Substituting Equation 2 into 3, ω_3 can be calculated by:

$$\omega_3 = \frac{z_2 z_1}{z_3 z_2}\omega_1 = \frac{z_1}{z_3}\omega_1 = i\omega_1 \quad \text{(Equation 4)}$$

where i is the transmission ratio; in the swing extension phase, the drive shaft and the one-way bearing are engaged. The rotor rotates with the drive shaft, and its speed ω can be written as:

$$\omega = \omega_3 \quad \text{(Equation 5)}$$

Thus, the relationship between rotor speed and angular velocity of knee joint rotation can be obtained as:

$$\omega = i\omega_0 \quad \text{(Equation 6)}$$

From Equation 6, the rotor speed is positively related to the gear train's transmission ratio and the rotational angular speed of the human knee. At this time, since this paper uses the electromagnetic conversion method, the output voltage is written as the following equation:

$$E = nNBL^*v = nNBL^*\omega R \quad \text{(Equation 7)}$$

where n and N represent the number and turns of coils, respectively. R is the radius of the rotor, L^* represents the coils' effective length, and B represents the magnetic flux density. The output current I can be given as:

$$I = \frac{E}{R_i + R_0} = \frac{nNBL^*\omega R}{R_i + R_0} \quad \text{(Equation 8)}$$

where R_i and R_o are the resistance of coils and the load resistance of the system, respectively.

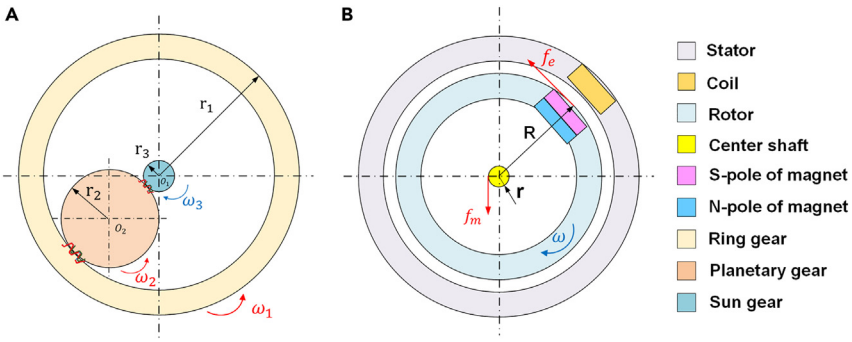

Figure 5. Motion transfer analysis and dynamic modeling of the NKEH

(A) Operating schematic of the planetary gear train.

(B) The dynamic model of the energy conversion module.

Based on the homo-phase transfer mechanism, the NKEH is driven by the knee joint rotation to generate electricity in the swing extension phase. The system has no mechanical energy input and the device relies on the rotatory inertia of the rotor to generate electricity in the standing and swing flexion phases, and the output voltage depends on the rotor's rotational speed. Figure 5B is the dynamic model of the energy conversion module in NKEH; the rotation process is mainly subjected to the magnetic moment M_e and the frictional moment M_m, and M_e can be expressed as:

$$M_e = f_e R \quad \text{(Equation 9)}$$

where R is the radius of the rotor and f_e represents the electric-magnetic damping force which depends on the magnetic field and induced current:

$$f_e = NBIL^* \quad \text{(Equation 10)}$$

Substituting Equation 8 into 10, f_e can be written as:

$$f_e = \frac{nN^2B^2L^{*2}\omega R}{R_i+R_0} \quad \text{(Equation 11)}$$

The frictional moment M_m can be expressed as:

$$M_m = f_m r \quad \text{(Equation 12)}$$

where r is the radius of the drive shaft and f_m is the damping force; it can be expressed as the product of the rotational damping factor c^*, mass, and angular velocity in rotational motion:

$$f_m = mc^*\omega \quad \text{(Equation 13)}$$

The rotor rotates around the central axis and the rotation equation can be expressed as:

$$M = J\dot{\omega} \quad \text{(Equation 14)}$$

where J represents the moment of inertia of the rotor and M represents the torque on the rotor, mainly including the magnetic torque and the friction torque so that M can be expressed as the sum of M_e and M_m.

$$M = M_e + M_m \quad \text{(Equation 15)}$$

Substituting 9, 11, 12, and 13 into Equation 15, M then can be written as:

$$M = \frac{nN^2B^2L^{*2}\omega R^2}{R_i+R_0} + mc^*\omega r \quad \text{(Equation 16)}$$

Substituting Equation 16 into 14, the expression of rotational angular acceleration $\dot{\omega}$ can be obtained:

$$\dot{\omega} = \frac{\frac{nN^2B^2L^{*2}\omega R^2}{R_i+R_0} + mc^*\omega r}{J} \quad \text{(Equation 17)}$$

Therefore, the rotor's angular velocity of rotation under the effect of rotational inertia can be expressed as:

$$\omega_{(t)} = \omega - \dot{\omega}t \quad \text{(Equation 18)}$$

In this phase, the output voltage of NKEH is:

$$E_{(t)} = nNBL^{*}\omega_{(t)}R \quad \text{(Equation 19)}$$

Substituting Equation 17 and Equation 18 into 19, $E_{(t)}$ can be written as:

$$E_{(t)} = nNBL^{*}R\left(\omega - \frac{\frac{nN^{2}B^{2}L^{*^{2}}\omega R^{2}}{R_i+R_0}+mc^{*}\omega r}{J}t\right) \quad \text{(Equation 20)}$$

In the swing extension phase, the output power of NKEH P_1 can be given as:

$$P_1 = I^{2}R_0 = \left(\frac{nNBL^{*}\omega R}{R_i+R_0}\right)^{2}R_0 \quad \text{(Equation 21)}$$

During the rotor inertia drive phase, the output power of the NKEH P_2 can be given as:

$$P_2 = \frac{E_{(t)}^{2}}{R_0} = \frac{\left[nNBL^{*}R\left(\omega - \frac{\frac{nN^{2}B^{2}L^{*^{2}}\omega R^{2}}{R_i+R_0}+mc^{*}\omega r}{J}t\right)\right]^{2}}{R_0} \quad \text{(Equation 22)}$$

The above-mentioned analysis shows that various factors play a role in the output power of the system, including the parameter settings of the coils and magnets, the transmission ratio of the planetary wheel system, the external load, and the swing speed of the knee. Also, the system has no mechanical energy input in the stance phase and swing flexion phase and relies on the rotor inertia to generate power.

Simulation of the dynamic models

The energy conversion module is a key of the system; in this part, simulation software is used to optimize the design of the energy conversion module of the NKEH. Two energy conversion models are simulated and modeled using COMSOL Multiphysics dynamic modeling software. The first energy conversion model: the pole of two adjacent magnets is different. The second energy conversion model: the pole of two adjacent magnets is the same. Figures 6A and 6B show the magnetic field strengths of the two models. It can be visualized from the figure that the magnetic field strength is higher in the first model. Then, the output power was calculated using COMSOL Multiphysics software. Figures 6C and 6D show the two models' output curves at a speed of 240 r/min. The figure shows that the first conversion model's output power is 66 mW, while the output power of the second conversion model is only 6.8 mW. It is possible to conclude that the first energy conversion model has better output performance. Therefore, in the next experiments, this pole configuration is used.

Experiments details

In the experimental section, we first made a prototype of the NKEH. Figure 7A shows the overall structure and components of the prototype. The energy harvester is installed at the knee joint through two linkages, which are made of 6061 aluminum alloy with high strength and the planetary gear train, rotor, and stator are 3D printed using a lightweight resin material. In this paper, a small vibrating table is designed and manufactured to test the output performance of NKEH. The processing and assembly diagrams of the vibrating table are shown in Figures 7B and 7C. The structure diagram of the vibrating table is shown in Figure 7D. The vibrating table comprises a frame, a stud, a disk, two shafts, four axle seats, two linear bearings, two knuckle bearings, and a motor. The vibrating table converts the rotation of the motor into linear reciprocating vibration according to the crank-slider principle and realizes the frequency variation of vibration excitation by controlling the speed of the motor and the position of the disc connection hole.

Before conducting the NKEH energy collection experiment, we tested the stability and durability of the system under reciprocating motion. The vibration table provided the excitation, and the test conditions were set to the maximum operating condition (excitation frequency of 4 Hz and swing angle of 90°). After 72,000 reciprocating motions, we inspected the structure and function of the system. The results showed that the connecting rod, transmission mechanism, and power generation structure were not damaged, and the gear surface showed slight wear but did not affect the actual operation. At the same time, the power

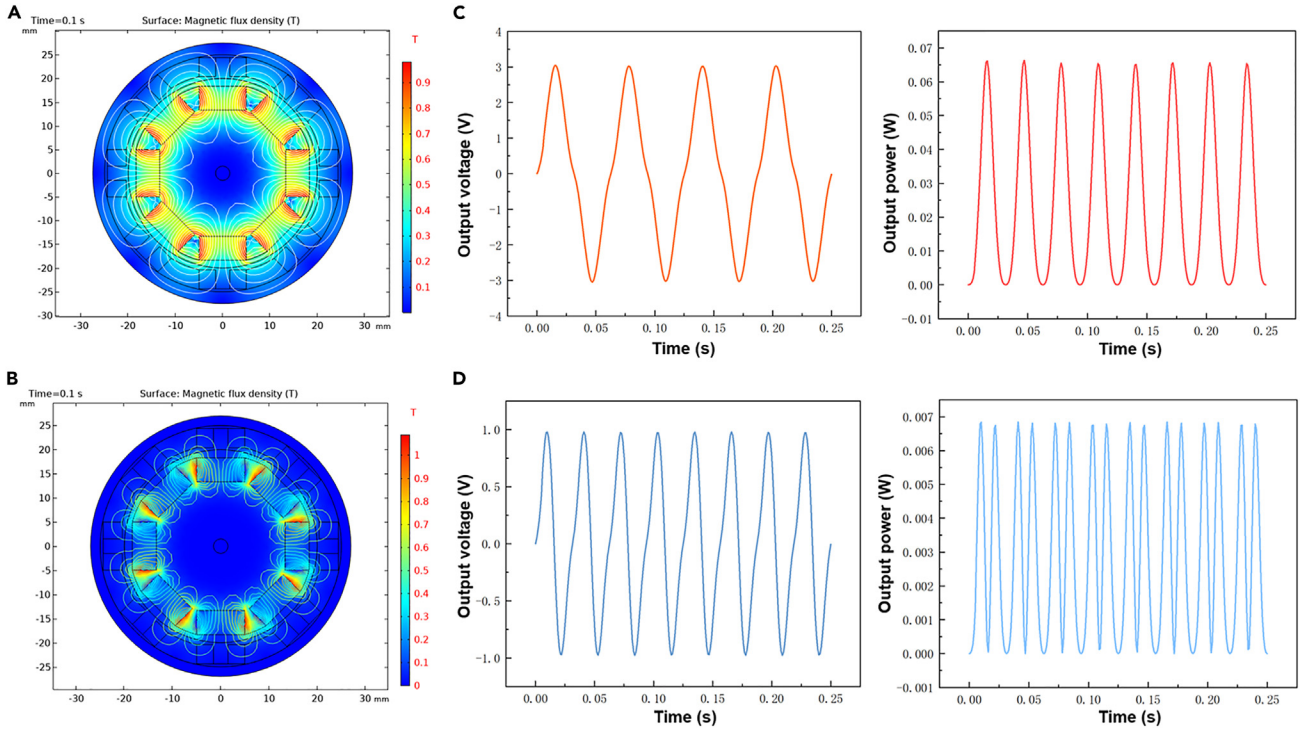

Figure 6. Simulation of the dynamic models

(A) Magnetic flue density of the first model.

(B) Magnetic flue density of the second model.

(C) Output curve of the first model.

(D) Output curve of the second model.

generation capacity of the NKEH did not decrease. Considering that human walking excitation is usually in the range of 1–2 Hz, the damage caused by the system is even smaller. Therefore, the stability and durability of the system meet practical usage requirements.

In the experimental part, vibrating table experiments were first conducted on NKEH, as shown in Figure 8. The NKEH is installed on the vibration table, the digital oscilloscope records the voltage signal of the energy collector, the resistance box is used to provide external load, and the USB disk is used to collect experimental data. The maximum excitation frequency in this part of the experiment is 4 Hz, and the maximum rotation angle is 90°. Then, we mounted the NKEH on the human knee and analyzed the output performance at walking and running conditions, and the application of the device was analyzed through the experimental data. Finally, we designed and conducted sensor power experiments to test the feasibility of the proposed NKEH to power the sensors.

RESULT AND DISCUSSION

Test on the vibrating table

In this section, we have conducted vibrating table test on the NKEH. The value of the load determines the output power; therefore, it is necessary to find the optimal load for the system. Load experiments were first carried out using a resistor box to adjust the external load, and the excitation frequency was adjusted to 1 Hz and the swing angle to 90°. Figures 9A and 9B show the output voltage waveforms, the specific output voltage value, and the output power value under different loads. It is obvious to see that the output voltage increases with increasing load, while the output power shows an increase and then decreases, reaching a maximum at a load of 160 Ω. Therefore, the optimal load for the NKEH is determined to be 160 Ω based on the experimental results.

Secondly, the effects of motion frequency and swing angle on the output performance of the NKEH were analyzed. The swing angle was set to 90° and the load resistance is set to the optimal resistor value of 160 Ω;

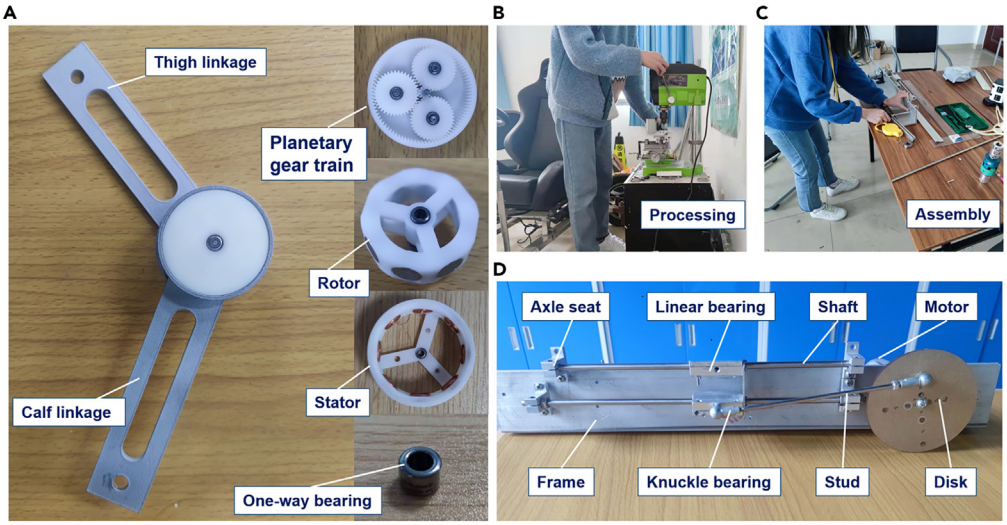

Figure 7. Prototype of the NKEH and schematic of the vibrating table

(A) Prototype and components of the NKEH.

(B) Processing of the vibrating table.

(C) Assembly of the vibrating table.

(D) Components of the vibrating table.

the NKEH's output characteristics were tested under different excitations conditions. Figure 9C illustrates the output voltage waveform, and Figure 10A shows the variation of output root-mean-square (RMS) voltage and output power of NKEH with increasing excitation frequency at a certain swing angle. The output RMS voltage and power of NKEH increased with the increase of frequency, and the minimum was 1.01 V and 6.35 mW, while the maximum was 5.22 V and 170.56 mW. Then, the excitation frequency was set to 2 Hz and the load resistance is set to the optimal resistor value of 160 Ω; the NKEH's output performance was tested at different swing angles. Figure 9D demonstrates the output voltage waveforms. The output RMS voltage and power of NKEH increased with the increase of swing angle, and the minimum was 0.52 V and 1.67 mW at the motion angle of 15°, and the maximum was 2.46 V and 37.70 mW at the motion angle of 90°, as shown in Figure 10B.

Figures 10C and 10D show the trends in output voltage and output power for different excitations, respectively. It can be seen that the RMS voltage and output power of the system increase with the swing angle,

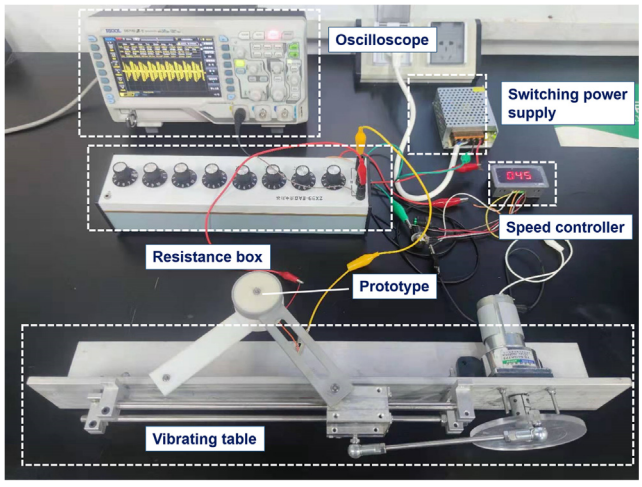

Figure 8. Schematic of the vibrating table experiment setup

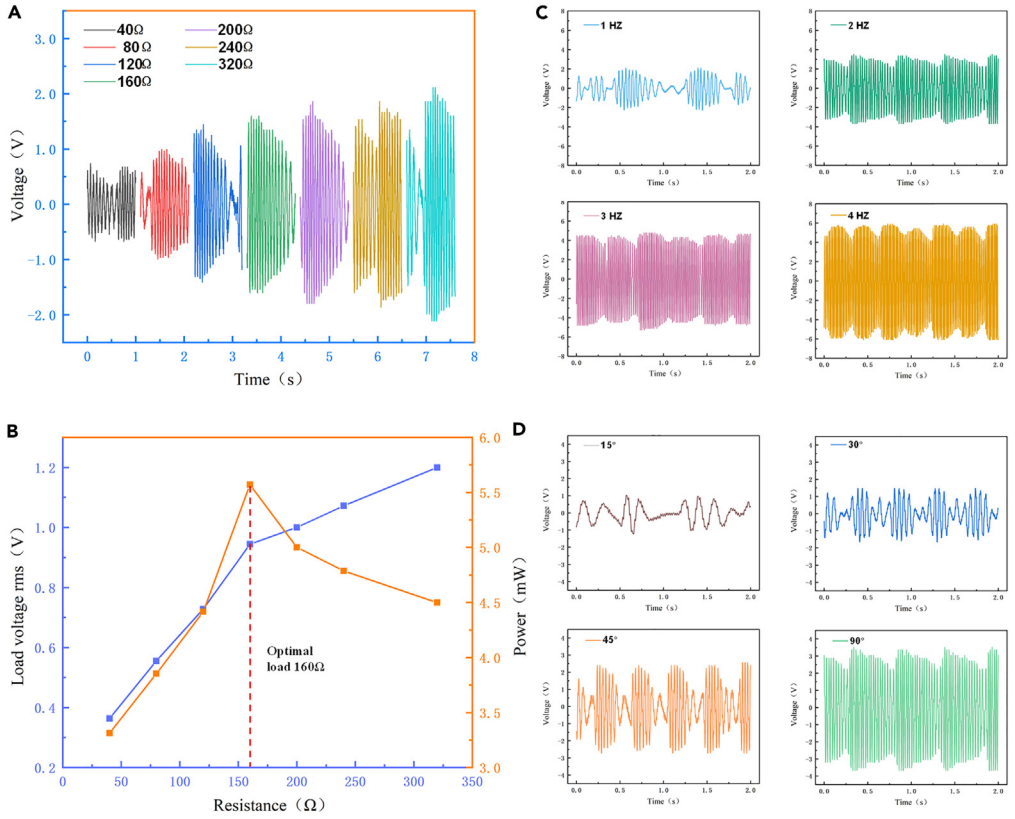

Figure 9. Output characteristics of the NKEH under the vibrating table-based experimental testing

(A) Voltage waveform under different resistances.

(B) Voltage and power under different resistances.

(C) Voltage waveform under different excitation frequencies at the optimal load.

(D) Output voltage waveform under different swing angles at the optimal load.

under the same excitation frequency. When the swing angle is the same, the RMS voltage and output power of the system increase with the increase of the excitation frequency. When the swing angle is 15° and the excitation frequency is 1 Hz, the RMS voltage and output power of the system are the minimum values, which are 0.25 V and 0.40 mW, respectively. When the swing angle is 90° and the excitation frequency is 4 Hz, the RMS voltage and output power of the system are the maximum values, which are 1.07 V and 170.56 mW, respectively. This leads to the following conclusions: The output performance of the NKEH increases as the excitation frequency and swing angle increase.

Human motion test

This part of the experiment was designed to investigate the NKEH's output properties at different motion excitation of the human body. The NKEH was mounted at the knee joint of the tester, as shown in Figure 11A. A resistor box provides an external load (set to 160 Ω) and uses an oscilloscope to record the output voltage signal. In order to more comprehensively simulate the daily activities of people, three human movement states are set: running, level walking, and downhill walking. Figure 11B shows the output performance of NKEH under different human motion states. The output RMS voltage is 0.62 V, while the output power is 2.41 mW when the tester is level walking.

In contrast, when the tester walks downhill, the RMS voltage and power are 0.72 V and 3.24 mW, respectively. This is because the knee does more negative muscles work in a downhill walking state, which is consistent with previous scholarly studies. When the tester runs, the knee joint oscillation angle and frequency increase significantly compared to walking, so the NKEH has better output performance.

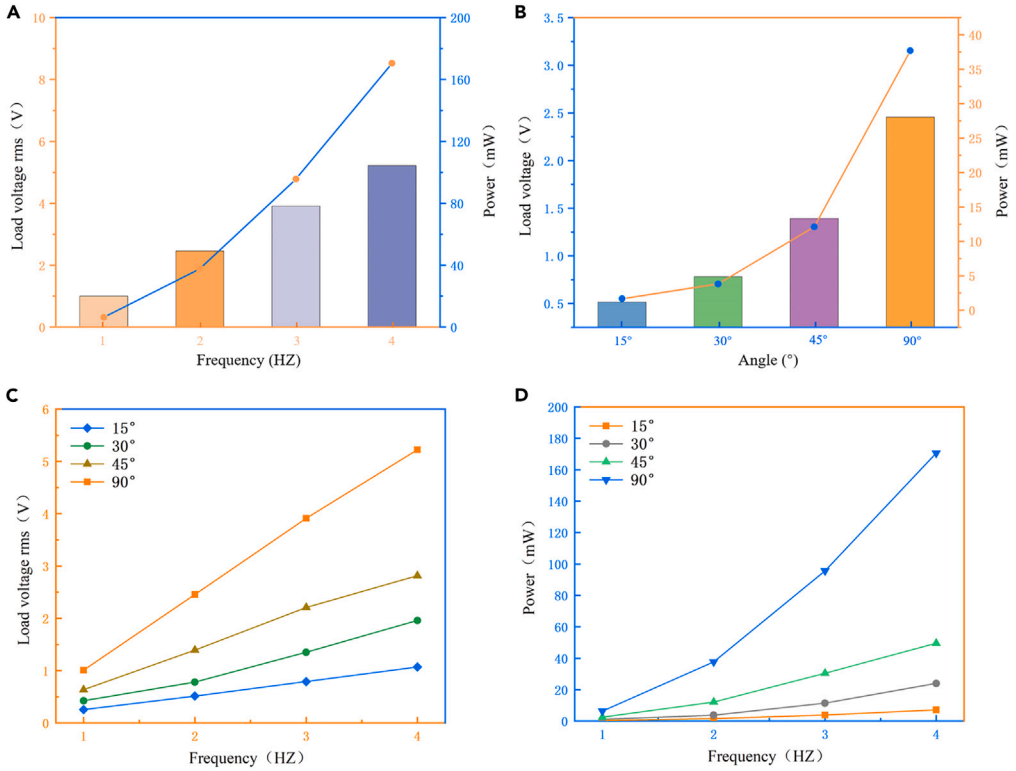

Figure 10. Vibrating table-based experimental results

(A) Output performance at different motion frequencies.

(B) Output performance at different swing angles.

(C) Variation curves of output RMS voltage.

(D) Output power variation curves.

Application of the NKEH

Figure 11C shows that the proposed NKEH provides energy to the wearable health monitoring device by harvesting the knee-negative muscle work. Wearable health monitoring devices mainly consist of various monitoring sensors, Table 3 lists the types and power of some commonly used health monitoring sensors. A wearable health monitoring device typically consists of three modules: the monitoring sensor module, the communication module, and a power management circuit module. Usually, the power management circuit is always on, and the sensor and communication modules are intermittently turned on. Assuming that the sensor reading time is 1 ms, the interval of sensor reading data is 1s, so the actual working time of the sensor is 86.4 s per day. Similarly, the size of the data read each time is assumed to be 1 byte. When the data transmission speed is 10 kbps, the actual working time of the transmission module is only 8.64 s as shown in Table 4.

The human test experiment, as mentioned previously, demonstrates that the output power of NKEH is different in different human movement states. Therefore, the daily power generation can be estimated by analyzing the movement state of humans. Assuming that the user of NKEH walks 8000 steps per day with a stride length of 0.65 m and speed of 1.2 m/s, after calculation, we can get the daily walking time of 1.2 h for users. Considering that people rarely run under normal circumstances, it is assumed that the daily running time of the human body is only 0.15 h. The daily sleep time is assumed to be 8 h, except for the above state; the rest of the time is regarded as no movement state. On this basis, the one-day power generation of the NKEH installed on the human body can be obtained. As shown in Table 5, the NKEH can generate about 17.40 J of energy a day, while the total daily power consumption of the human health monitoring device is about 13.55 J, which indicates that the NKEH designed in this paper can provide sufficient electricity for the health monitoring device.

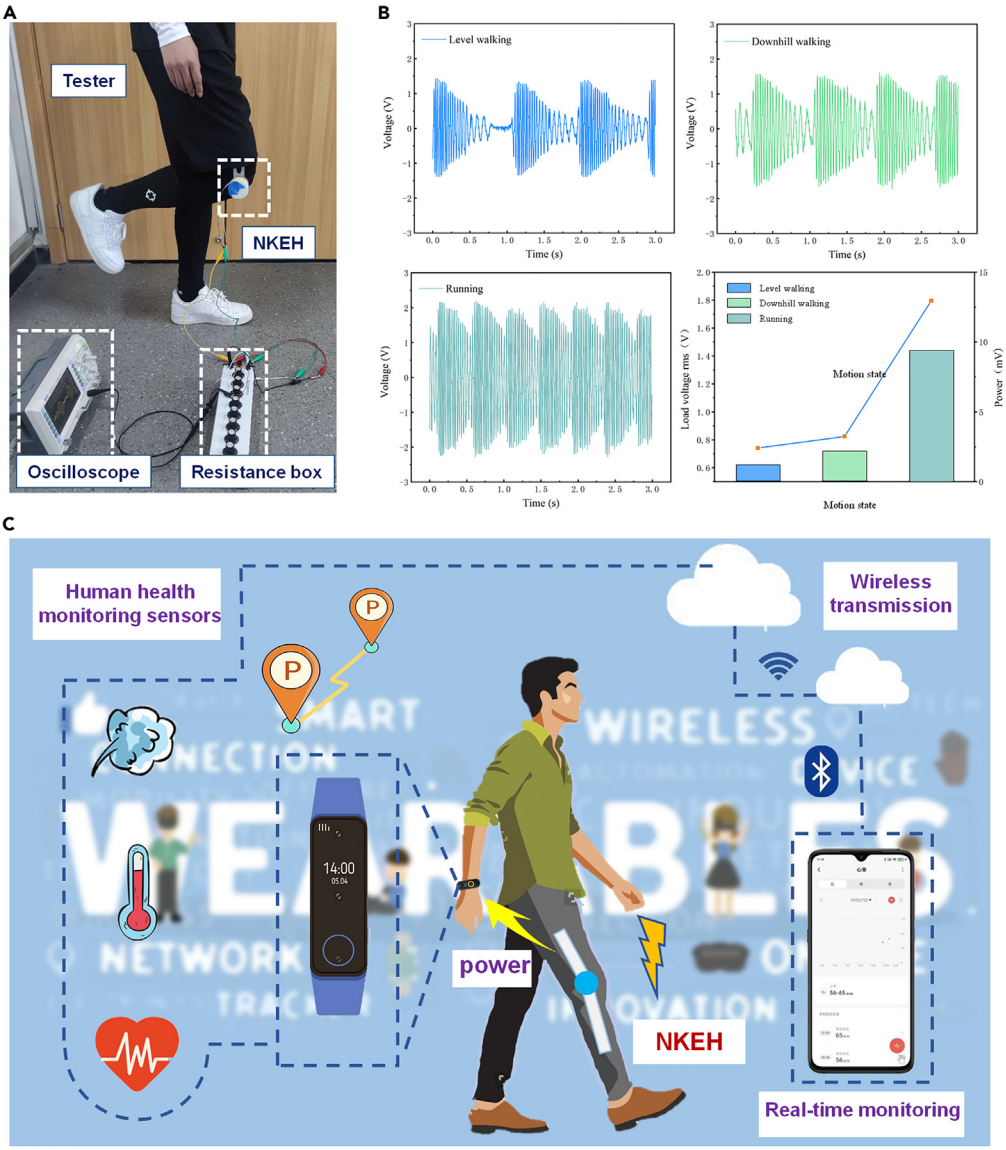

Figure 11. Human movement experiments and applications of the NKEH

(A) Experiment setup.

(B) The NKEH's output performance under different motion excitation.

(C) Applications of the NKEH.

Finally, the sensor power supply-based experiments were performed. The test experiment's overall layout and the circuit's partial schematic are shown in Figures 12A and 12B. The AC-DC converter is used to realize the AC-DC current conversion; the booster module increases the voltage, and a supercapacitor is used to release and store the power for this sensor power supply experiment. Firstly, a capacitor charging experiment was conducted under human motion excitation. Figure 12C shows the voltage change curves when charging different capacitors (220, 470, 1000, and 2200 μF). It can be seen from the figure that the voltage of the small capacitor rises faster, and the energy harvester can charge a 220 μF capacitor from 0 to 4 V in just 3 s. As the capacitance of the capacitor increases, the charging speed slows down and the maximum voltage of the capacitor decreases accordingly. According to the energy storage formula of the capacitor: $E = CU^2/2$, the energy stored in the capacitor during the charging process can be calculated. Taking a 220 μF capacitor as an example, the energy stored in the capacitor can be calculated as $2.75*10^{-3}$ J. Based on the energy storage theory of the capacitor, the electrical heat generated during the charging process is equal to the energy stored in the capacitor, which is $2.75*10^{-3}$ J. At this point, the output power of the energy harvesting

Table 3. Typical health monitoring sensor types and power

Type	Power (mW)
GPS sensor	75
Blood pressure sensors	25
Temperature sensor	1.8
Breathing sensors	15
Humidity sensor	0.2
Heart rate monitoring sensor	20

machine is 2.1 mW, and the charging time is 3 s. Therefore, the energy input to the energy collector is W = Pt = $6.2*10^{-3}$ J. It can be calculated that the electrical heat loss during the charging process is 44.35%, and the circuit energy loss is 11.3%. Meanwhile, to test the practical application of NKEH, a temperature and humidity sensor power supply test was conducted, as shown in Figure 12D. By using NKEH to charge a supercapacitor to drive a wireless temperature and humidity sensor, after 150 s, NKEH successfully drove the normal operation of the sensor. After 200 s, the system successfully drove the sensor Bluetooth module, allowing users to view sensor data on their mobile phones, demonstrating the huge potential of NKEH in wireless monitoring applications for human body.

Comparison of typical joint energy harvesters

This paper proposes a full negative-work knee energy harvester based on the homo-phase transfer mechanism, which is designed to operate in sync with the biological characteristics of human walking. Table 6 provides a comprehensive comparison of the proposed energy harvester for lower limbs with existing counterparts in terms of various factors such as joint positions, mass or size, power generation, and working mechanism. Compared to [25] and [26], the proposed energy harvester operates solely during the negative work phase of a human's walking cycle, thereby reducing any supplementary metabolic load. Moreover, the proposed energy harvester has a significant enhancement in power generation compared to [25], [26], and [47], allowing it to meet the power requirements of microbiological sensors. While [38] and [48] have achieved higher power generation during the negative work phase, they employ a potentiometer and sensors to detect the knee joint angle, which is an unnecessary power-consuming process. Furthermore, the prototypes of [38] and [48] are weighty, more than 1 kg, and do not prioritize the user's comfort, potentially disrupting their daily activities. In contrast, the proposed harvester has a total weight of only 0.17 kg, providing minimal interference to the wearer. Furthermore, this study avoids using energy-consuming potentiometers or sensors, indicating that all the energy harvested can be fully utilized to power a wearable health monitoring device.

Conclusions

In this paper, we propose a full NKEH based on the homo-phase transfer mechanism. Unlike the traditional human energy harvester, the proposed NKEH only harvests knee-negative work and does not harvest knee-positive work. Also, this paper controls the transmission of motion and power generation based on the homo-phase transfer mechanism instead of using potentiometers. Using the COMSOL Multiphysics dynamic modeling software to optimize the design of the energy conversion module and the optimal magnetic pole combination model is obtained. To test the output performance of the NKEH and the effectiveness of powering wearable health detection devices, we designed the test bench and conducted experiments. First, we analyzed the NKEH's output performance at different excitation conditions; the output performance was positively correlated with the motion frequency and the swing angle. Then, we wore the

Table 4. Power consumption of health monitoring devices

Type	Power (mW)	Time (s)	Consumption (J)
Monitoring sensors	137	86.4	12.25
Communications	60	8.64	0.52
Power management	0.009	86400	0.78
Total	–	–	13.55

Table 5. The amount of electricity generated by the NKEH one day

State	Time (h)	Power (mW)	Daily power generation (J)
Running	0.15	12.95	6.99
Motionless	14.65	0	0
Walking	1.2	2.41	10.41
Sleeping	8.0	0	0
Total			17.40

NKEH on the human knee joint and conducted different human motion excitation experiments. The output power was 3.24 mW when the tester was downhill walking, which is increased compared to the output power of 2.41 mW during downhill walking, and the output power of the NKEH was substantially increased when the tester was running, which could reach 12.95 mW. Finally, the practical application of the proposed NKEH was analyzed, and the calculated results showed that the NKEH worn on a human could generate 17.40 J/day power, which can satisfy the normal operation of a typical health monitoring device. In conclusion, the proposed NKEH can generate large sustainable electrical energy without extra effort from the human body, showing great potential to realize self-powering of human health monitoring equipment.

Limitations of the study

This paper proposes a full negative-work knee energy harvester that is specifically designed to power human health monitoring equipment and does not cause significant disturbance to the human movement. However, given the limitations of our experimental equipment and technical conditions, there are still some areas that require further improvement in future research endeavors.

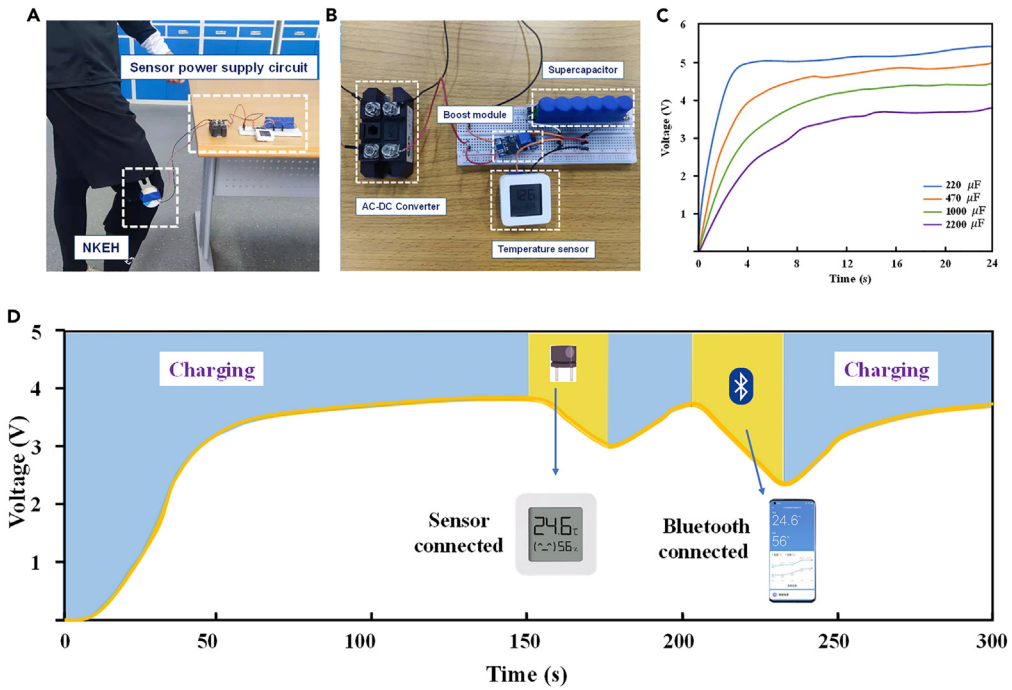

Figure 12. Sensor power supply experiment of the NKEH

(A) Overall experimental setup.

(B) Partial experimental setup.

(C) Charging different capacitors.

(D) Temperature and humidity sensor power supply test.

Table 6. Comparison of typical joint energy harvesters

Research	Joint	Weight or sizes	Power	Mechanism	Negative work phase
Romero[26]	Ankle	2.0 cm^3	0.43 mW	Micro-rotation	No
Donelan[38]	Knee	1.6 kg	4.8 W	Potentiometer	Yes
Ibrahim[47]	Knee	19.24 cm^2	58 μW	Triboelectric	Yes
Shepertycky[48]	Knee	1.06 kg	0.25 W	Sensors	Yes
Dai[25]	Hip	126.8 cm^3	0.28 mW	Rotary motor	No
This paper	Knee	0.17 kg	12.95 mW	One-way bearing	Yes

(1) In this study, we have focused on utilizing the homo-phase transfer mechanism to harvest a significant amount of negative work during the swing extension phases of knee oscillation. However, it is important to note that there may be a small amount of negative work during other stages of the human gait cycle that have not been utilized in our paper. Future research should pay close attention to this aspect.

(2) Moreover, it is worth noting that due to the limitations of our experimental equipment, we were unable to test the metabolic capacity of our subjects in this study. Further research in this area is required to advance our understanding and knowledge in this field.

STAR★METHODS

Detailed methods are provided in the online version of this paper and include the following:

- KEY RESOURCES TABLE
- RESOURCE AVAILABILITY
  - Lead contact
  - Material availability
  - Data and code availability
- EXPERIMENTAL MODEL AND SUBJECT DETAILS
- METHODS DETAILS
- QUANTIFICATION AND STATISTICAL ANALYSIS

SUPPLEMENTAL INFORMATION

Supplemental information can be found online at https://doi.org/10.1016/j.isci.2023.107011.

ACKNOWLEDGMENTS

This work was supported by the National Natural Foundation of China under Grants No. 51975490 and by the Science and Technology Projects of Sichuan under Grants Nos. 23QYCX0280, 2022JDRC0075 and 2022NSFSC0461; and by the Science and Technology Projects of Yibin under Grant No. SWJTU2021020001 and SWJTU2021020002; and by the Science and Technology Projects of Chengdu under Grant No. 2021YF0800138GX.

AUTHOR CONTRIBUTIONS

H.Z.: Conceptualization, Methodology, Validation, Software, Writing-Original draft; H.W.: Data curation, Investigation, Validation, Writing-Original draft; Z.Z.: Supervision, Resources, Writing-Review; Y.P.: Supervision, Resources, Writing-Review; X.L.: Data curation, Investigation.

DECLARATION OF INTERESTS

The author declares no competing interests.

Received: April 3, 2023
Revised: May 9, 2023
Accepted: May 27, 2023
Published: June 5, 2023

REFERENCES

1. Zhu, M., Yu, J., Li, Z., and Ding, B. (2022). Self-healing fibrous membranes. Angew Chem. Int. Ed. Engl. *61*, e202208949. https://doi.org/10.1002/anie.202208949.

2. Liu, C., Zhang, B., Chen, W., Liu, W., and Zhang, S. (2021). Current development of wearable sensors based on nanosheets and applications. TrAC, Trends Anal. Chem. *143*, 116334. https://doi.org/10.1016/j.trac.2021.116334.

3. Pu, X., An, S., Tang, Q., Guo, H., and Hu, C. (2021). Wearable triboelectric sensors for biomedical monitoring and human-machine interface. iScience *24*, 102027. https://doi.org/10.1016/j.isci.2020.102027.

4. Zhu, M., Li, J., Yu, J., Li, Z., and Ding, B. (2022). Superstable and intrinsically self-healing fibrous membrane with bionic confined protective structure for breathable electronic skin. Angew Chem. Int. Ed. Engl. *61*, e202200226. https://doi.org/10.1002/anie.202200226.

5. Cai, S., Xu, C., Jiang, D., Yuan, M., Zhang, Q., Li, Z., and Wang, Y. (2022). Air-permeable electrode for highly sensitive and noninvasive glucose monitoring enabled by graphene fiber fabrics. Nano Energy *93*, 106904. https://doi.org/10.1016/j.nanoen.2021.106904.

6. Wei, X., Zhu, M., Li, J., Liu, L., Yu, J., Li, Z., and Ding, B. (2021). Wearable biosensor for sensitive detection of uric acid in artificial sweat enabled by a fiber structured sensing interface. Nano Energy *85*, 106031. https://doi.org/10.1016/j.nanoen.2021.106031.

7. Zhang, S., Xia, Q., Ma, S., Yang, W., Wang, Q., Yang, C., Jin, B., and Liu, C. (2021). Current advances and challenges in nanosheet-based wearable power supply devices. iScience *24*, 103477. https://doi.org/10.1016/j.isci.2021.103477.

8. Zhang, S., Liu, C., Sun, X., and Huang, W. (2022). Current development of materials science and engineering towards epidermal sensors. Prog. Mater. Sci. *128*, 100962. https://doi.org/10.1016/j.pmatsci.2022.100962.

9. Sun, X., Sun, X., Wang, Q., Wang, X., Feng, L., Yang, Y., Jing, Y., Yang, C., and Zhang, S. (2022). Biosensors toward behavior detection in diagnosis of alzheimer's disease. Front. Bioeng. Biotechnol. *10*, 1031833. https://doi.org/10.3389/fbioe.2022.1031833.

10. Cai, J., Du, M., and Li, Z. (2022). Flexible temperature sensors constructed with fiber materials. Adv. Mater. Technol. *7*, 2101182. https://doi.org/10.1002/admt.202101182.

11. Tsikriteas, Z.M., Roscow, J.I., Bowen, C.R., and Khanbareh, H. (2021). Flexible ferroelectric wearable devices for medical applications. iScience *24*, 101987. https://doi.org/10.1016/j.isci.2020.101987.

12. Zhang, S., Zhou, Y., Liu, Y., Wallace, G.G., Beirne, S., and Chen, J. (2021). All-polymer wearable thermoelectrochemical cells harvesting body heat. iScience *24*, 103466. https://doi.org/10.1016/j.isci.2021.103466.

13. Chen, J., and Wang, Z.L. (2017). Reviving vibration energy harvesting and self-powered sensing by a triboelectric nanogenerator. Joule *1*, 480–521. https://doi.org/10.1016/j.joule.2017.09.004.

14. Cui, X., Huang, F., Zhang, X., Song, P., Zheng, H., Chevali, V., Wang, H., and Xu, Z. (2022). Flexible pressure sensors via engineering microstructures for wearable human-machine interaction and health monitoring applications. iScience *25*, 104148. https://doi.org/10.1016/j.isci.2022.104148.

15. Lin, P.H., Chang, W.L., Sheu, S.C., and Li, B.R. (2020). A noninvasive wearable device for real-time monitoring of secretion sweat pressure by digital display. iScience *23*, 101658. https://doi.org/10.1016/j.isci.2020.101658.

16. Zhou, M., Al-Furjan, M.S.H., Zou, J., and Liu, W. (2018). A review on heat and mechanical energy harvesting from human – principles, prototypes and perspectives. Renew. Sustain. Energy Rev. *82*, 3582–3609. https://doi.org/10.1016/j.rser.2017.10.102.

17. Al-Nabulsi, J., El-Sharo, S., Salawy, N., and Al-Doori, H. (2019). Methods of energy generation from the human body: a literature review. J. Med. Eng. Technol. *43*, 255–272. https://doi.org/10.1080/03091902.2019.1658818.

18. Yin, L., Moon, J.-M., Sempionatto, J.R., Lin, M., Cao, M., Trifonov, A., Zhang, F., Lou, Z., Jeong, J.-M., Lee, S.-J., et al. (2021). A passive perspiration biofuel cell: high energy return on investment. Joule *5*, 1888–1904. https://doi.org/10.1016/j.joule.2021.06.004.

19. Martin, J.-P., and Li, Q. (2019). Design, model, and performance evaluation of a biomechanical energy harvesting backpack. Mech. Syst. Signal Process. *134*, 106318. https://doi.org/10.1016/j.ymssp.2019.106318.

20. Chen, X., Wu, Y., Shao, J., Jiang, T., Yu, A., Xu, L., and Wang, Z.L. (2017). On-skin triboelectric nanogenerator and self-powered sensor with ultrathin thickness and high stretchability. Small *13*, 1702929. https://doi.org/10.1002/smll.201702929.

21. Renaud, M., Fiorini, P., van Schaijk, R., and van Hoof, C. (2012). Corrigendum: harvesting energy from the motion of human limbs: the design and analysis of an impact-based piezoelectric generator. Smart Mater. Struct. *21*, 049501. https://doi.org/10.1088/0964-1726/21/4/049501.

22. Huang, T., Wang, C., Yu, H., Wang, H., Zhang, Q., and Zhu, M. (2015). Human walking-driven wearable all-fiber triboelectric nanogenerator containing electrospun polyvinylidene fluoride piezoelectric nanofibers. Nano Energy *14*, 226–235. https://doi.org/10.1016/j.nanoen.2015.01.038.

23. Yan, B., Zhang, C., and Li, L. (2018). Magnetostrictive energy generator for harvesting the rotation of human knee joint. AIP Adv. *8*, 056730. https://doi.org/10.1063/1.5007195.

24. Gao, F., Liu, G., Chung, B.L.-H., Chan, H.H.-T., and Liao, W.-H. (2019). Macro fiber composite-based energy harvester for human knee. Appl. Phys. Lett. *115*, 033901. https://doi.org/10.1063/1.5098962.

25. Dai, D., and Liu, J. (2014). Hip-mounted electromagnetic generator to harvest energy from human motion. Front. Energy *8*, 173–181. https://doi.org/10.1007/s11708-014-0301-2.

26. Romero, E. (2011). Rotational energy harvester for body motion. In IEEE 24th international conference on micro electro mechanical systems, *2011*.

27. Chen, C., Ibekwe-SanJuan, F., and Hou, J. (2010). The structure and dynamics of cocitation clusters: a multiple-perspective cocitation analysis. J. Am. Soc. Inf. Sci. Technol. *61*, 1386–1409. https://doi.org/10.1002/asi.21309.

28. Chen, Y.M.A., Liang, S.Y., Shih, Y.P., Chen, C.Y., Lee, Y.M., Chang, L., Jung, S.Y., Ho, M.S., Liang, K.Y., Chen, H.Y., et al. (2006). CiteSpace II: detecting and visualizing emerging trends and transient patterns in scientific literature. J. Clin. Microbiol. *44*, 359–365. https://doi.org/10.1002/asi.20317.

29. Zhou, N., Hou, Z., Zhang, Y., Cao, J., and Bowen, C.R. (2021). Enhanced swing electromagnetic energy harvesting from human motion. Energy *228*, 120591. https://doi.org/10.1016/j.energy.2021.120591.

30. M Turab, N., Abu Owida, H., I Al-Nabulsi, J., Abu-Alhaija, M., I Al-Nabulsi, J., and Abu-Alhaija, M. (2022). Recent techniques for harvesting energy from the human body. Comput. Syst. Sci. Eng. *40*, 167–177. https://doi.org/10.32604/csse.2022.017973.

31. Sharghi, H., and Bilgen, O. (2023). Dynamics of pendulum-based systems under human arm rotational movements. Mech. Syst. Signal Process. *183*, 109630. https://doi.org/10.1016/j.ymssp.2022.109630.

32. Collins, S.H., Wiggin, M.B., and Sawicki, G.S. (2015). Reducing the energy cost of human walking using an unpowered exoskeleton. Nature *522*, 212–215. https://doi.org/10.1038/nature14288.

33. Liu, M., Qian, F., Mi, J., and Zuo, L. (2022). Biomechanical energy harvesting for wearable and mobile devices: state-of-the-art and future directions. Appl. Energy *321*, 119379. https://doi.org/10.1016/j.apenergy.2022.119379.

34. Simpson, C.S., Welker, C.G., Uhlrich, S.D., Sketch, S.M., Jackson, R.W., Delp, S.L., Collins, S.H., Selinger, J.C., and Hawkes, E.W. (2019). Connecting the legs with a spring improves human running economy. J. Exp. Biol. *222*, jeb202895. https://doi.org/10.1242/jeb.202895.

35. Mooney, L.M., Rouse, E.J., and Herr, H.M. (2014). Autonomous exoskeleton reduces metabolic cost of human walking. J. NeuroEng. Rehabil. *11*, 151.

36. Mooney, L.M., Rouse, E.J., and Herr, H.M. (2014). Autonomous exoskeleton reduces metabolic cost of human walking during load carriage. J. NeuroEng. Rehabil. *11*, 80.

37. Nuckols, R.W., Takahashi, K.Z., Farris, D.J., Mizrachi, S., Riemer, R., and Sawicki, G.S. (2020). Mechanics of walking and running up and downhill: a joint-level perspective to guide design of lower-limb exoskeletons. PLoS One *15*, e0231996. https://doi.org/10.1371/journal.pone.0231996.

38. Donelan, J.M., Li, Q., Naing, V., Hoffer, J.A., Weber, D.J., and Kuo, A.D. (2008). Biomechanical energy harvesting: generating electricity during walking with minimal user effort. Science *319*, 807–810. https://doi.org/10.1126/science.1149860.

39. Xie, L., Li, X., Cai, S., Huang, G., and Huang, L. (2019). Knee-braced energy harvester: reclaim energy and assist walking. Mech. Syst. Signal Process. *127*, 172–189. https://doi.org/10.1016/j.ymssp.2019.03.008.

40. Ren, L., Cong, M., Zhang, W., and Tan, Y. (2021). Harvesting the negative work of an active exoskeleton robot to extend its operating duration. Energy Convers. Manag. *245*, 114640. https://doi.org/10.1016/j.enconman.2021.114640.

41. Shepertycky, M., and Li, Q. (2015). Generating electricity during walking with a lower limb-driven energy harvester: targeting a minimum user effort. PLoS One *10*, e0127635. https://doi.org/10.1371/journal.pone.0127635.

42. Chan, H.H.-T., Gao, F., Chung, B.L.-H., Liao, W.-H., and Cao, J. (2021). Knee energy harvester with variable transmission to reduce the effect on the walking gait. Smart Mater. Struct. *30*. https://doi.org/10.1088/1361-665X/ac0bfe.

43. Liu, M., Hughes-Oliver, C., Queen, R., and Zuo, L. (2021). Comparison of negative-muscle-work energy harvesters from the human ankle: different designs and trade-offs. Renew. Energy *170*, 525–538. https://doi.org/10.1016/j.renene.2021.01.151.

44. Liu, M. (2018). Energy harvesting from ankle generating electricity by harvesting negative work. SMASIS2018.

45. Malcolm, P., Derave, W., Galle, S., and De Clercq, D. (2013). A simple exoskeleton that assists plantarflexion can reduce the metabolic cost of human walking. PLoS One *8*, e56137. https://doi.org/10.1371/journal.pone.0056137.

46. WINTE, D.A. (1983). Energy generation and absorption at the ankle and knee during fast, natural, and slow cadences. Clin. Orthop. Relat. Res.

47. Armbruster, P., Oster, Y., Vogt, M., and Pylatiuk, C. (2017). Design of a mechanism for converting the energy of knee motions by using electroactive polymers. Biomed. Tech. *62*, 643–652. https://doi.org/10.1515/bmt-2016-0138.

48. Shepertycky, M., Burton, S., Dickson, A., Liu, Y.F., and Li, Q. (2021). Science_Sarah Burton_Removing energy with an exoskeleton reduces the metabolic cost of walking. Science *372*, 957–960.

STAR★METHODS

KEY RESOURCES TABLE

REAGENT or RESOURCE	SOURCE	IDENTIFIER
Software and algorithms		
Microsoft Visio 2019	Microsoft	https://www.microsoft.com/zh-cn/microsoft-365/visio/flowchart-software
Origin 2018	Originlab	https://www.originlab.com/
COMSOL Multiphysics 5.5	COMSOL	https://cn.comsol.com/
Other		
DS1102Z-E digital oscilloscope	RIGOL	https://rigol.com

RESOURCE AVAILABILITY

Lead contact

Further information and requests for resources and reagents should be directed to and will be fulfilled by the lead contact Zutao Zhang (zzt@swjtu.edu.cn).

Material availability

This study did not generate new unique reagents.

Data and code availability

- All data reported in this paper will be shared by the lead contact upon reasonable request.
- This paper does not report original code.
- Any additional information required to reanalyze the data reported in this paper is available from the lead contact upon request.

EXPERIMENTAL MODEL AND SUBJECT DETAILS

In the **Human motion test** and **Application of the NKEH**, the experimenter was an adult male (25 years of age) in good health with a normal level of movement. There was no physical or physiological discomfort after completion of the Human Energy Harvesting experiment. The experimenter provided written informed consent prior to participation. The experimental procedures were approved by the School of Mechanical Engineering, Southwest Jiaotong University. The experiment took 120 to 150 min to complete and participants were compensated for their time (200RMB).

METHODS DETAILS

All methods can be found in the text, please check the **Human walking and homo-phase transfer mechanism** for the starting point of System design. Please check the **System design** for structural design. Please check the **MODELLING AND ANALYSIS** for theoretical models and simulations of the system. Please check the **EXPERIMENTS DETAILS** for prototyping and setting up experiments. Please check the **Application of the NKEH** to know the application potential of the device. Using Microsoft Visio 2019 to generate visual images in the manuscript. Origin 2018 was used to process experimental data and generate visual images in the manuscript. The dynamic modeling software COMSOL Multiphysics 5.5 was used to simulate the magnetic field distribution. The oscilloscope (RIGOL DS1102) is used to evaluate the output characteristics of the equipment. In addition, a presentation video is provided to more vividly introduce the whole paper, as shown in video S1.

QUANTIFICATION AND STATISTICAL ANALYSIS

Microsoft Visio 2019 is used to generate the visual images in the manuscript. Origin 2018 is used to process experimental data and generate visual images in the manuscript. The dynamic modeling software COMSOL Multiphysics 5.5 is used to simulate magnetic flux distribution and magnet force. The voltage signals are captured by the digital oscilloscope (RIGOL DS1102).